nature geoscience

SUPPLEMENTARY INFORMATION

DOI: 10.1038/NGEO3053

In the format provided by the authors and unedited.

Contribution of topographically-generated submesoscale turbulence to Southern Ocean overturning

Xiaozhou Ruan[1], Andrew F. Thompson[1], Mar M. Flexas[1] & Janet Sprintall[2]

[1]*Environmental Science & Engineering, California Institute of Technology*

[2]*Scripps Institution of Oceanography, University of California, San Diego*

Supplementary material

1. Estimates for water mass transformation rates:

The water mass transformation rate can be expressed, following Marshall et al. (1999), using a diapycnal velocity $\tilde{\mathbf{e}}$, as

$$T = -\int\int_A \tilde{\mathbf{e}} \cdot \mathbf{n}_b \, dA = \int\int_A \frac{\nabla \cdot \mathbf{F}_b}{|\nabla b|} dA. \tag{1}$$

Here $b = -g\left(\rho - \rho_0\right)/\rho_0$ is the buoyancy and ρ_0 is a reference density, A is the area of a buoyancy surface across which the diapycnal transport is measured, $\mathbf{n}_b$ is the unit vector normal to the isopycnal and $\mathbf{F}_b$ is the turbulent buoyancy flux. It has been argued that the vertical buoyancy flux scales with the dissipation rate as $\Gamma\epsilon$, where Γ is the mixing efficiency (Osborn 1980). Thus, the buoyancy flux divergence can be estimated as $\Gamma\epsilon/h$ where h is the thickness of the bottom mixed layer (BML); this assumes that the buoyancy flux vanishes at the solid bottom. Using a mixing efficiency $\Gamma = 0.2$, a typical bottom mixed layer thickness $h = 100$ m and a local vertical stratification $N^2 = \frac{\partial b}{\partial z} = 10^{-6} s^{-2}$, the diapycnal velocity can be estimated as 2×10^{-4} m s^{-1}, or $\sim$20 m day^{-1}. Considering a 5 km-wide boundary current (associated with the southern boundary of the

ACC) that flows along the continental slope for a distance of 500 km in southern Drake Passage (Fig. S4; Orsi *et al*. 1995), A is 2.5×10^9 m^2. Using equation (5), this yields a local water mass transformation rate of 0.5 Sv. We acknowledge that the mixing efficiency, Γ, is uncertain in this area, nevertheless, this likely remains an underestimate since only the shear-induced mechanism is accounted for here.

The use of the vertical buoyancy gradient N^2 assumes that the diapycnal mixing and associated water mass modification is a local, one-dimensional (vertical) process, which relies on the rapid export of modified water into the interior. McDougall and Ferrari (2017) hypothesize that water masses may be modified and upwell in boundary layers over sloping topography. In this case, N^2 should be replaced by the lateral buoyancy gradient across the continental slope. Estimating this value across multiple glider sections gives a value of roughly 5×10^{-8} s^{-2} (Fig. 1c). This smaller buoyancy gradient suggests a local diapycnal velocity 20 times larger than the previous estimate using the vertical buoyancy gradient. We note that the lateral buoyancy gradient is a more challenging quantity to estimate, especially if the incropping of density surfaces is heterogeneous along the slope (see, for instance, Fig. 4 in Thompson and Heywood, 2008). Now we estimate the area of relevant buoyancy surfaces A within the BML using the BML thickness of 100 m and a longitudinal distance of 500 km along Southern Drake Passage which yields $A = 5 \times 10^7$ m^2. The water mass transformation rate can be thus estimated to be 0.2 Sv. It is important to note that, according to the hypothesis, the excessive (upwelling) diapycnal volume flux along the bottom boundary layers has to be largely compensated by diapycnal downwelling in the stratified mixed layers globally. While the estimates above are associated with some uncertainty, they are

sufficiently large to warrant further investigation.

2. Extrapolation to the circumpolar Southern Ocean using numerical model output:

In order to estimate the circumpolar relevance of the proposed mechanism, we turn to output from a high-resolution global numerical model to examine the interactions between ACC fronts and major topographic features in the Southern Ocean.

LLC4320 is a global ocean and sea ice simulation that represents full-depth ocean processes. The simulation is based on a Latitude/Longitude/polar-Cap (LLC) configuration of the MIT general circulation model (MITgcm; Marshall *et al.* 1997; Hill *et al.* 2007). The LLC grid has 13 square tiles with 4320 grid points on each side (hereafter called LLC4320) and 90 vertical levels for a total grid count of 2:21010. Horizontal grid spacing ranges from 0.75 km near Antarctica to 2.2 km at the Equator and vertical levels have 1-m thickness near the surface to better resolve the diurnal cycle. The simulation is initialized from a data-constrained global ocean and sea ice solution provided by the Estimating the Circulation and Climate of the Ocean, Phase II (ECCO2) project (Menemenlis *et al.* 2005, 2008; Losch *et al.* 2010), and includes atmospheric pressure and tidal forcing (Menemenlis *et al.* 2014). The inclusion of tides allows for successful reproduction of shelf-slope dynamics and water mass modification (Flexas *et al.* 2015). Surface boundary conditions are from the European Center for Medium-Range Weather Forecasts (ECMWF) atmospheric operational model analysis, starting in 2011. The sections shown in Figure S4 correspond to a snapshot of LLC4320 on 29/11/2011.

Assuming that there are strong interactions between deep-reaching ACC currents and sloping

bottom topography near the Kerguelen Plateau, Campbell Plateau, Drake Passage and ridges and fracture zones in the South Pacific and Atlantic, as seen in Figure S4, then a conservative estimate for A in equation (5) would be 2.5×10^{10} m^2 (an average of 5km-wide narrow front is assumed). This area estimation would yield a global transformation of LCDW of 5 Sv for the local vertical process. For the along-bottom diapycnal upwelling framework, we estimate the area A to be 5×10^8 m^2 which yields a transformation rate of 2 Sv (with the possible compensating downwelling neglected).

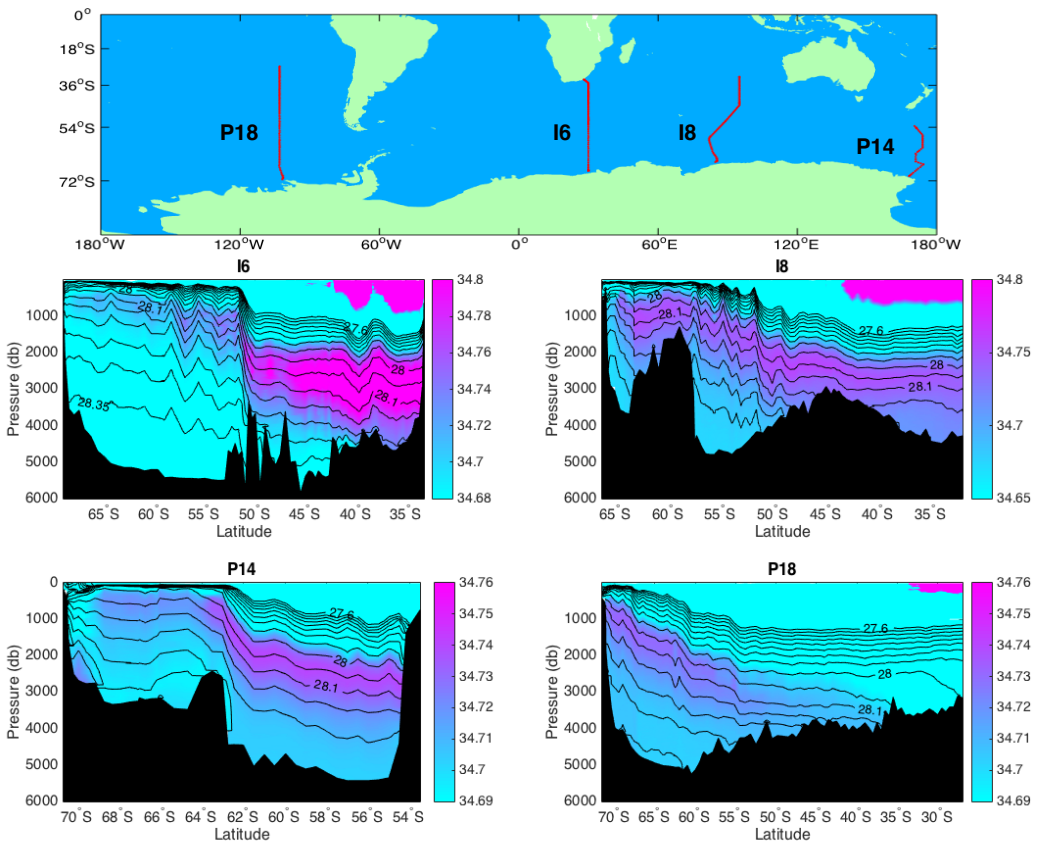

Figure S1: Salinity distributions from WOCE transects (summer measurements) I6, I8, P14 and P18 (Orsi and Whitworth 2005). The purple colors highlight that Lower Circumpolar Deep Water (characterized by a salinity maximum) incrops on the Antarctic continental slope and deeper topographic features broadly around Antarctica. Neutral density surfaces are indicated as black contours.

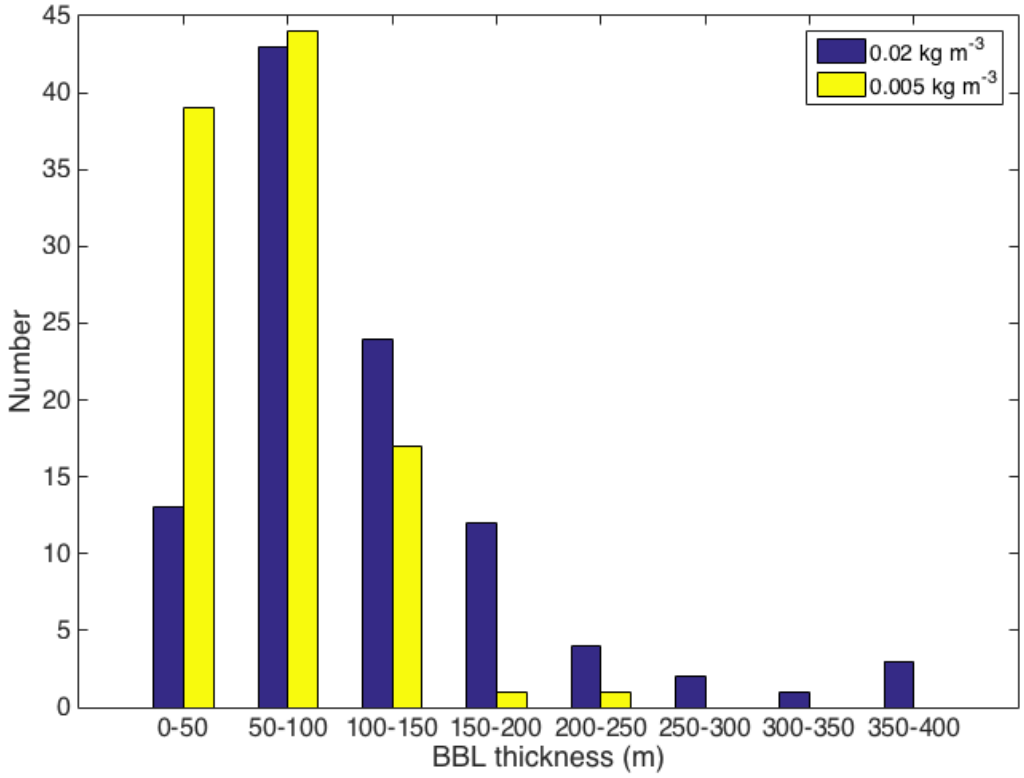

Figure S2: Statistics of bottom mixed layer (BML) thickness (m) based on a Δ 0.02 kg m^{-3} threshold (blue) and a Δ 0.005 kg m^{-3} threshold (yellow).

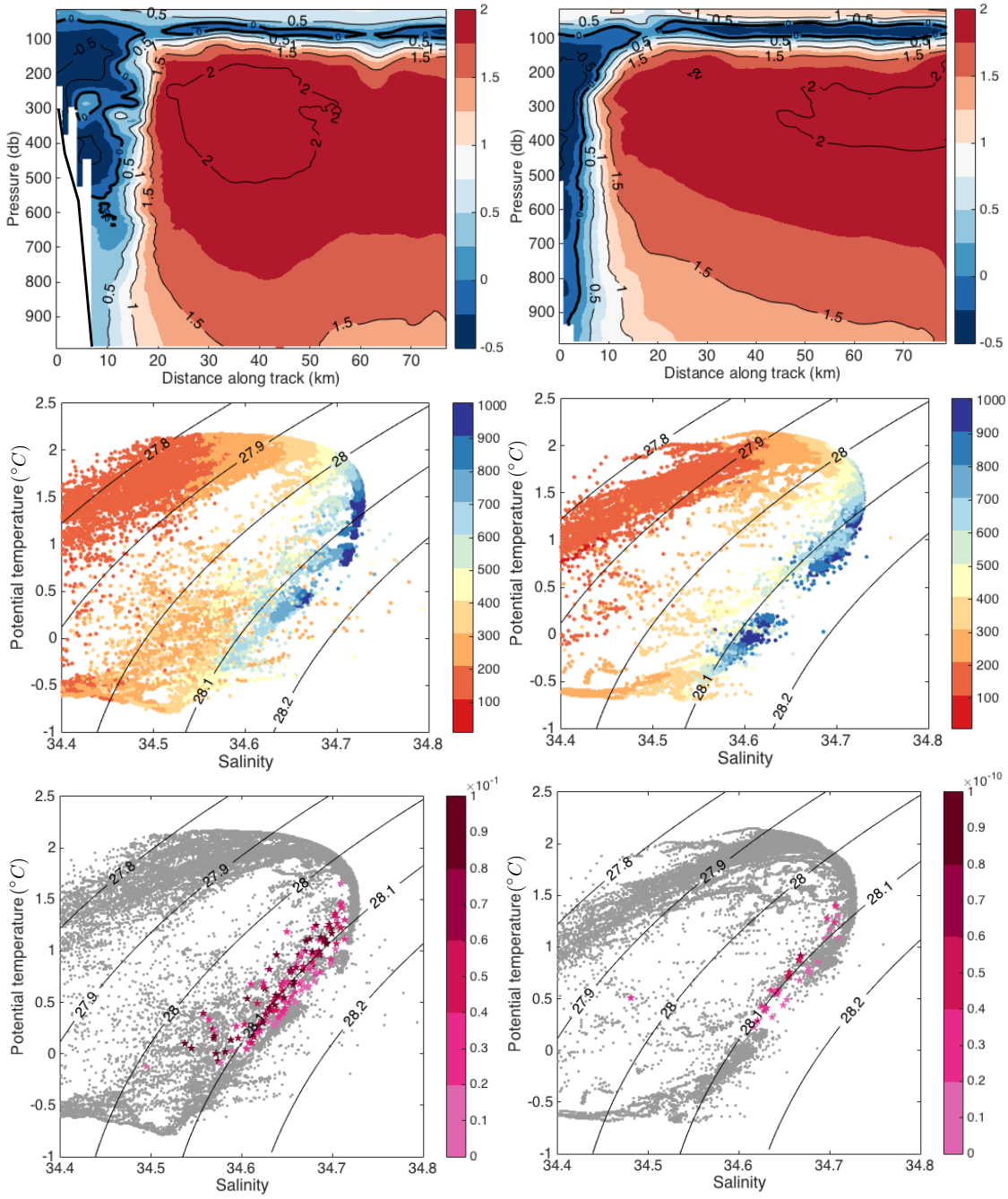

Figure S3: Two transect examples of CDW being close to (left panels; Transect 5) and away from (right panels; Transect 8) the slope. (Upper panels) Potential temperature sections. Isothermals are labeled every 0.5°C. The 2°C contour roughly defines the location of the

Bdy. The 0°C isotherm (in bold black) marks the front separating warm CDW from cold shelf water. (Middle panels) Θ/S diagram of glider data colored by depth (in meters). (Lower panels) Positive Ertel PV (in magenta) over all data sampled for each given transect (in gray).

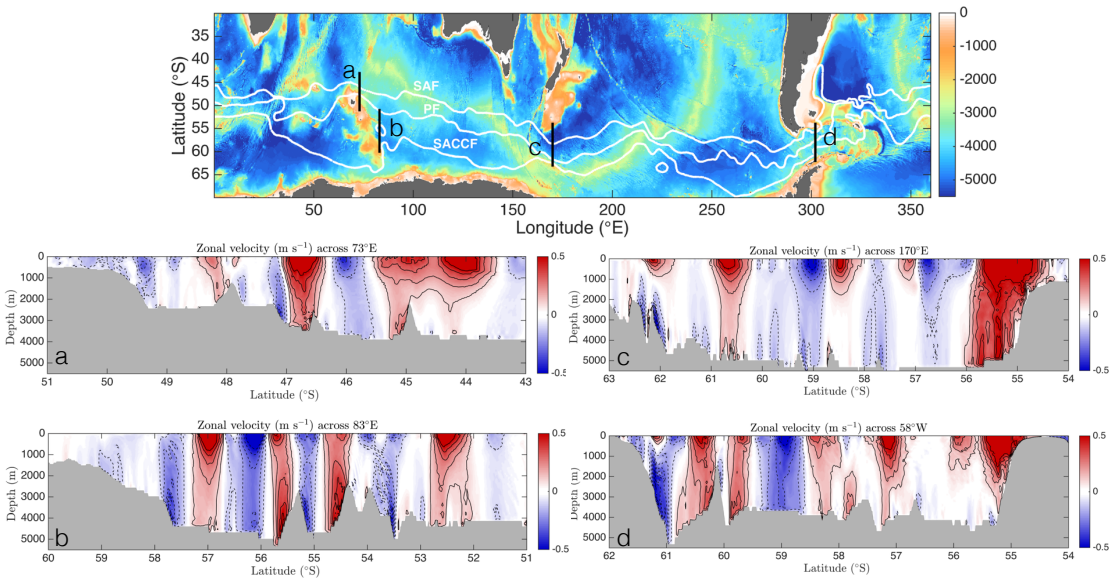

Figure S4: Zonal velocity snapshots across topographic features in the Southern Ocean from a high-resolution numerical model (See model introduction in Supplementary Material). Transects a, b, c and d correspond to Northern and Southern Kerguelen Plateau, Campbell Plateau (including the Macquarie Ridge) and Drake Passage. White contours in the upper panel are the climatological frontal positions in the Southern Ocean (Orsi *et al*. 1995) and black straight lines correspond to the transects from which zonal velocity snapshots are shown below. Black contours in the lower four panels are zonal velocities (eastward, positive, solid lines). Contour levels are from 0.1m/s to 0.5m/s with a 0.1m/s interval. Deep-reaching fast boundary currents (some with bottom velocity intensification) interacting with sloping topography can be seen widely in the Southern Ocean across the chosen major topographic features.

References:

Flexas, M. M., et al. Role of tides on the formation of the Antarctic Slope Front at the Weddell-Scotia Confluence. *J. Geophys. Res.*, **120**, 3658–3680 (2015).

Hill, C., et al. Investigating solution convergence in a global ocean model using a 2048-processor cluster of distributed shared memory machines. *Sci. Prog.*, **15**, 107–115 (2007).

Losch, M., et al. On the formulation of sea-ice models. Part 1: Effects of different solver implementations and parameterizations. *Ocean Modell.*, **33**, 129–144 (2010).

Marshall, J., D. Jamous, and J. Nilsson. Reconciling thermodynamic and dynamic methods of computation of water-mass transformation rates. *Deep-Sea Res. I*, **46**, 545–572 (1999).

McDougall, T. J., and R. Ferrari. Abyssal upwelling and downwelling driven by near-boundary mixing. *J. Phys. Oceanogr.*, **47**, 261–283 (2017).

Marshall, J., et al. A finite-volume, incompressible Navier Stokes model for studies of the ocean on parallel computers. *J. Geophys. Res.*, **102**, 5753–5766 (1997).

Menemenlis, D., et al. ECCO2: High resolution global ocean and sea ice data synthesis. *Mercator Ocean Q. News.*, **31**, 13–21 (2008).

Menemenlis, D., et al. NASA supercomputer improves prospects for ocean climate research. *Eos, Trans. AGU*, **86**, 89–96 (2005).

Menemenlis, D., et al. "Global llcXXXX simulations with tides." Presentation at annual ECCO meeting (2014), avail. at http://ecco2.org/meetings/2014/Jan_MIT/presentations/ThursdayPM/05_menemenlis.pdf.

Orsi, A. H., T. Whitworth, and W. D. Nowlin. On the meridional extent and fronts of the Antarctic Circumpolar Current. *Deep-Sea Res. I*, **42**, 641–673 (1995).

Orsi, A. H. and Whitworth III, T. Hydrographic Atlas of the World Ocean Circulation Experiment (WOCE): Volume 1: Southern Ocean (WOCE International Project Office, 2005).

Osborn, T. R. Estimates of the local rate of vertical diffusion from dissipation measurements. *J. Phys. Oceanogr.*, **10**, 83–89 (1980).

Thompson, A. F., and K. J. Heywood. Frontal structure and transport in the northwestern Weddell Sea. *Deep-Sea Res. I*, **55**, 1229–1251 (2008).